



Enhancing Pool Boiling Heat Transfer by Structured Surfaces– A Lattice Boltzmann Study

Y. Huang¹, Y. Tian², W. Ye¹, W. Li¹, J. Lei¹ and Y. Zhang^{1†}

¹ School of Mechatronics Engineering, Nanchang University, Nanchang, Jiangxi, 330031, China

² Institute of Energy and Sustainable Development (IESD), School of Engineering and Sustainable Development, De Montfort University, Leicester LE1 9BH, England, UK

†Corresponding Author Email: yzhan2033@163.com

(Received February 18, 2021; accepted August 17, 2021)

ABSTRACT

The structured surface-enhanced pool boiling process and associated heat transfer enhancement characteristics are numerically investigated by using the pseudopotential multiphase flow lattice Boltzmann (LB) model coupled finite difference method (FDM). In the current study, the effects of different microstructure geometries (square structures, triangular serrated structures, triangular-raised structures) and varying spacing in triangular-raised structures ($d = 0, 22, 44, 66, 88, 110$ l.u. (lattice units)) on boiling heat transfer (BHT) characteristics and bubble dynamics behavior are studied in detail. The results showed that microstructure can accelerate bubble nucleation. Among the three microstructures, the heat transfer performance of triangular-raised structures was significantly better than that of square and triangular serrated structures in the nucleate boiling (Ja number is 0.124-0.145). The oscillation and deformation of bubbles led to the lateral migration of bubbles, the continuous nucleation of small bubbles. The phenomenon of re-wetting of heating surface occurred in the process of bubble migration, necking, deformation and detachment was found, which enhances heat transfer in nucleate boiling. At the same time, the growth, oscillation and detachment of bubbles also perturb the liquid and enhance the natural convection around the bubbles. Therefore the main BHT mechanism of nucleate boiling on the three kinds of structured surface is the combined action of transient heat conduction and micro-convection. The variation of the spacing between microstructures showed an important effect on the BHT performance of the heating surface and the generation of activated nucleation sites in the nucleate boiling. Triangular-raised structures can enhance transient heat conduction and micro-convection, with the strongest enhancement effect at $d = 66$ l.u. when the Ja number is 0.124.

Keywords: Boiling; Structured surface; Bubble dynamics; Lattice Boltzmann method.

NOMENCLATURE

a	a parameter in P-R state equation	T_c	critical temperature
b	a parameter in P-R state equation	T_h	temperature of the center three grids on the bottom wall
c	lattice speed	T_s	saturation temperature
c_s	lattice sound speed of the D2Q9 model	\mathbf{u}	macroscopic velocity
c_v	specific heat at constant volume	u_x	velocity in the x direction
d	distance between microstructure	u_y	velocity in the y direction
D_0	initial droplet diameter	w_i	weights
D_1	stable droplet diameter	x	spatial position
D_d	droplet detachment diameter	(x_0, y_0)	central coordinate of the computing domain
e_i	discrete velocity in the i direction		
f_i	density distribution function	Greek symbols	
f_i^{eq}	density equilibrium distribution function	δ_t	time step
\mathbf{F}	total force	ΔT	superheat on the heating surface
\mathbf{F}_b	fluid-solid pseudopotential interaction force	θ	equilibrium contact angles at the saturation temperature
F_i^*	forcing term within the velocity space	κ	acentric factor
\mathbf{F}_f	buoyancy force	ρ	macroscopic density

F_m	fluid-fluid pseudopotential interaction force	ρ_L	macroscopic density of the liquid
F_x	total force in the x direction	ρ_V	macroscopic density of the vapor
F_y	total force in the y direction	σ	a parameter that can tune the condition of the mechanical stability
g	gravitational acceleration	τ	relaxation time
G	strength of fluid-fluid interaction	ν_L	kinematic viscosity of the liquid
G_w	a parameter that can align the interaction force	ν_V	kinematic viscosity of the vapor
h_{lv}	specific latent heat of fluid	χ	thermal diffusion coefficient
I	unit tensor	ψ	pseudopotential
J	heat transfer coefficient	ω_i	weight coefficient in the fluid-solid pseudopotential interaction force
Ja	Jacob number		
L_x	length of computation domain		
L_y	width of computation domain		
L_w	total length of heating surface		
M	non-orthogonal transformation matrix of D2Q9 model		
m	density distribution function of the moment space	EOS	equation of state
m^{eq}	density equilibrium distribution function of the moment space	h	high
O	forcing term in the moment space	i	direction in a lattice
P_{EOS}	non-ideal equation of state	L	liquid
p_c	critical pressure	s	saturation
Q_{ave}	average heat flux	v	volume
R	a parameter in P-R state equation	V	vapor
r_0	droplet radius	x	x direction
S	a diagonal relaxation matrix	y	y direction
t	time	z	z direction
T	temperature		
T^t	temperature in t time		
$T^{t+\delta t}$	temperature in $t+\delta t$ time		
T_b	temperature on the heating surface		
λ	thermal conductivity		
		Subscripts	
		ave	average
		c	critical
		eq	equilibrium
		EOS	equation of state
		h	high
		i	direction in a lattice
		L	liquid
		s	saturation
		v	volume
		V	vapor
		x	x direction
		y	y direction
		z	z direction
		Abbreviations	
		FDM	Finite Difference Method
		LB	Lattice Boltzmann
		l.u.	Lattice units

1. INTRODUCTION

Nucleate boiling is an efficient way to transfer heat, which takes away significant latent heat through the generated bubbles, thus dissipating large heat fluxes. Because of its excellent heat dissipation capacity, it is widely used in engineering and industrial fields, such as nuclear reactors, power plants, electronic equipment cooling, refrigeration and chemical process (Dhir *et al.* 2013; Hamzekhani *et al.* 2015). In the early studies of boiling, researchers have conducted many experiments to study the boiling heat transfer (BHT) mechanism, the boiling phenomena, the boiling curve and so on, with some significant progress made (Wei *et al.* 2005; Chu *et al.* 2012). These developments have deepened our understanding of the boiling process and solved some problems in engineering and industrial fields. Thereupon many technologies were proposed to enhance the heat transfer performance of nucleate boiling. Among them, the surface modification technology has been widely used due to its high potential to enhance the heat transfer performance by providing larger surface area, higher nucleation site density and potentially smaller phase transition overheating (Thiagarajan *et al.* 2015). Surface

modification technology has been commonly adopted in two methods: one is to control the wettability of the boiling surface (Jo *et al.* 2011), and the other is to implement micro-nano machining on the boiling surface (Kim *et al.* 2015a).

The physical mechanism of boiling on structured surface is complex, which involves the dynamics of interaction between vapor, liquid, the solid heating surface and a series of complex phenomena such as flow field disturbance. Therefore, many experiments have been conducted to study the BHT mechanism and the physical phenomena in the boiling process (Xie *et al.* 2021a, 2021b, 2020; Zonouzi *et al.* 2018, Halon *et al.* 2018; Kim *et al.* 2015; Tang *et al.* 2016). Xie *et al.* (2021a) designed experiments to investigate the pool boiling heat transfer characteristics of multi-oriented hierarchical structured surfaces. The results showed that nanostructured surfaces exhibit better boiling performance than all multi-oriented planar surfaces. The departure time and fully developed vapor film thickness of the inclined surfaces increased with increasing surface orientation. Halon *et al.* (2018) designed two different kinds of enhanced boiling surfaces: NTS (narrow tunnel structure) and TS (tunnel structure), and studied the low-pressure

boiling phenomenon and BHT performance of these two structured surfaces. Their results indicated that the BHT performance of tunnel structure was significantly improved at lower pressure, at even one order of magnitude higher than that of a flat surface. [Kim *et al.* \(2015b\)](#) performed an experimental study on the effect of structured surface on BHT characteristics. Their results revealed that with the increase of surface roughness, the BHT performance increased but the enhancement slowed down gradually. [Tang *et al.* \(2016\)](#) designed a porous interconnected micro-channel network structured surface, and carried out a BHT performance research on the prepared surface. The results showed that the channel width had a significant effect on the BHT coefficient.

In boiling research, it is not sufficient enough to just rely on the experimental method because the experimental results are often contradictory due to complexity, many factors affecting the boiling curve are indistinguishable in the experimental study ([Jo *et al.* 2011](#); [O'hanley *et al.* 2013](#)). For the boiling of structured surfaces, there are certain limitations in the experimental research, such as the experimental cost, the manufacturing accuracy of structured surface, the accurate observation of bubble motion ([Dong *et al.* 2020](#)), etc. Therefore, numerical simulation has become an important means to investigate the potential BHT mechanism and characteristics involved in the boiling process on structured surfaces. The Lattice Boltzmann (LB) method is a mesoscopic method based on kinetic equations, and in recent year has received extensive attention in simulating complex fluid systems such as two-phase flow and vapor-liquid phase transition, having shown great potential ([Dong *et al.* 2020](#); [Zhao *et al.* 2021, 2019a, 2019b](#); [Chang *et al.* 2019](#); [Zhang *et al.* 2020](#); [Zhou *et al.* 2019](#); [Bi *et al.* 2019](#)). [Dong *et al.* \(2020\)](#) performed research on the BHT characteristics and bubble dynamics behavior during subcooled boiling on an inclined surface using lattice Boltzmann method. The effects of inclination angle and surface geometry on bubble motion and BHT performance were discussed in detail. The results showed that the BHT coefficient was not only related to the inclination angle, but also to the surface geometry. [Zhao *et al.* \(2021\)](#) studied the effect of confined space and free outlet boundary on the heat transfer characteristics of nucleation boiling under conjugate heat transfer using phase change lattice Boltzmann method. The obvious sliding growth phenomenon and curved rising trajectory and large deformation of the rising vapor bubble were observed in their study. [Chang *et al.* \(2019\)](#) used the thermal two-phase LB model to numerically simulate the enhanced BHT characteristics on the columnar structured surface. The effects of column height, column width and spacing on the BHT performance were analyzed in detail. The results revealed that the BHT performance mainly depends on the heating area and the local convection flow field. [Zhou *et al.* \(2019\)](#) used the LB model with two-particle distribution functions to study the bubble dynamic behavior during the boiling process of micro-pillar structured surface, including the periodic nucleation,

growth, and detachment process of bubbles, and analyzed in detail the effects of micro-pillar spacing and the height on bubble growth and detachment. The results showed that with the decrease of micro-pillar height, the heat flux increased and the departure period of nucleated bubbles shortened, while the spacing between two micro-pillars showed no distinct effect despite having great effect on the formation of activated nucleation sites. Although the LBM method has its own limitations that can not be well compared with the conditions used in experimental studies, from the above researchers using the LBM method and the conclusions drawn in the process of simulating boiling, the method can obtain the fine and detailed characterization of the bubble dynamics processes such as bubble nucleation, necking, deformation, merging and detachment and their effects on the boiling heat transfer characteristics, which is difficult to do in the experiment studies. Therefore, in the present study, the boiling heat transfer process of structured surface is qualitatively analyzed by using LBM method.

Previous studies have shown that micro-nano structured surfaces can significantly enhance BHT performance, and the geometric size, shape and spacing between structures have significant effects on BHT characteristics and bubble dynamics behavior in the boiling process. However, most of the numerical simulation studies on the influence factors of the geometric shape of the structured surface were to design various groove shapes on the structured surface to form stable nucleation sites, or to design the structural surface with a series of micro-pillars. There are few studies on the influence of raised structural surfaces of other shapes (such as triangular-raised structures formed by inclined heating surfaces), the mechanism and the effects of the spacing between the geometric structures on BHT characteristics and bubble dynamics behavior have not been fully understood. Therefore, the pool boiling process and the enhanced heat transfer characteristics of such structured surfaces are studied in the current study. A pseudopotential multiphase LB model coupled FDM proposed by [Li *et al.* \(2015\)](#) was adopted in the simulations. The model had been verified and employed successfully in several subsequent studies of pool boiling ([Li *et al.* 2015, 2018](#)). In the present work, the effects of the microstructure geometric shapes and the structure spacing on the bubble dynamic behavior and heat transfer characteristics are studied in detail, the phenomena during the boiling process are analyzed and the mechanism of heat transfer enhancement is revealed. The nucleation, growth, coalescence, detachment and rising of bubbles during the boiling process on the structured surface are presented. The distribution of heat flux with time and space on different structured surfaces are obtained and analyzed in detail. The current study can take a step forward the obtantion of a better revealing and understanding of the physical mechanisms behind the enhancement of heat transfer efficiency due to structured surfaces and the interaction between bubble dynamics and microstructure and its effect on boiling heat transfer characteristics.

2. NUMERICAL MODEL

In the current study, the pseudopotential multiphase flow LB model is applied to solve the gas-liquid two-phase flow problem in the boiling process, the two-phase density, the evolution of the interface, and the velocity variation within the flow field are obtained by solving the LB equation describing the density distribution function. The LB equation describing the density distribution function with multiple relaxation collision operators can be expressed as (Li *et al.* 2013)

$$f_i(\mathbf{x} + \mathbf{e}_i \delta_t, t + \delta_t) = f_i(\mathbf{x}, t) - (\mathbf{M}^{-1} \mathbf{S} \mathbf{M})_{ij} (f_j - f_j^{eq})_{(\mathbf{x}, t)} + \delta_t F_i^*(\mathbf{x}, t) \quad (1)$$

where f_i and f_i^{eq} are the function of density and density equilibrium distribution, respectively, \mathbf{x} is the spatial position, δ_t is the time step, \mathbf{M} is a transformation matrix with orthogonal property, \mathbf{e}_i is the discrete velocity in the i direction, F_i^* is the forcing term within the velocity space, \mathbf{S} is a diagonal matrix containing relaxation time, which is given by

$$\mathbf{S} = \text{diag}(\tau_0^{-1}, \tau_1^{-1}, \tau_2^{-1}, \tau_3^{-1}, \tau_4^{-1}, \tau_5^{-1}, \tau_6^{-1}, \tau_7^{-1}, \tau_8^{-1}) \quad (2)$$

The relaxation times are given by $\tau_0 = \tau_3 = \tau_5 = 1$, $\tau_1 = \tau_2 = 1.25$, $\tau_4 = \tau_6 = 1/1.1$ in the current study. The shear viscosity determines the relaxation time τ_7 and τ_8 ($\tau_7 = \tau_8$). Multiplying the orthogonal matrix \mathbf{M} , the right expression of equation 1 can be transformed into

$$\mathbf{m}^* = \mathbf{m} - \mathbf{S}(\mathbf{m} - \mathbf{m}^{eq}) + \delta_t (\mathbf{I} - 0.5\mathbf{S})\mathbf{O} \quad (3)$$

where $\mathbf{m} = \mathbf{M}\mathbf{f}$, $\mathbf{m}^{eq} = \mathbf{M}\mathbf{f}^{eq}$, $(\mathbf{I} - 0.5\mathbf{S})\mathbf{O} = \mathbf{M}\mathbf{F}^*$, \mathbf{I} and \mathbf{O} are the unit tensor and the forcing term within the moment space, respectively. The equilibria \mathbf{m}^{eq} can be written as follows:

$$\mathbf{m}^{eq} = \rho(1, -2 + 3|\mathbf{u}|^2, 1 - 3|\mathbf{u}|^2, u_x, -u_x, u_y, -u_y, u_x^2 - u_y^2, u_x u_y)^T \quad (4)$$

where ρ and \mathbf{u} are the macroscopic density and velocity, respectively. The macroscopic density and velocity can be obtained as follows:

$$\rho = \sum_i f_i, \quad \rho \mathbf{u} = \sum_i \mathbf{e}_i f_i + 0.5 \delta_t \mathbf{F} \quad (5)$$

where \mathbf{F} given by $\mathbf{F} = \mathbf{F}_m + \mathbf{F}_b + \mathbf{F}_f$ is the total force in the current study. \mathbf{F}_m and \mathbf{F}_b are the fluid-fluid and fluid-solid pseudopotential interaction force, respectively. \mathbf{F}_f is the buoyancy force. The interaction force \mathbf{F}_m is given by

$$\mathbf{F}_m = -G\psi(\mathbf{x}) \sum_i w_i \psi(\mathbf{x} + \mathbf{e}_i) \mathbf{e}_i \quad (6)$$

where G is the strength of fluid-fluid interaction, w_i and ψ are the weights and the pseudopotential, respectively. For the D2Q9 lattice, the weights are given as $w_{1-4} = 1/3$, $w_{5-8} = 1/12$. The pseudopotential is given by (Yuan and Schaefer 2006)

$$\psi(x) = \sqrt{\frac{2(p_{EOS} - \rho c_s^2)}{Gc^2}} \quad (7)$$

where c_s is the lattice speed in D2Q9 model, $c = 1$ is the lattice constant, and P_{EOS} is the non-ideal state equation. In the current study, the state equation of Peng-Robinson(P-R) is used (Yuan and Schaefer 2006)

$$P_{EOS} = \frac{\rho RT}{1 - b\rho} - \frac{a\phi(T)\rho^2}{1 + 2b\rho - b^2\rho^2} \quad (8)$$

$$\psi(T) = \left[1 + (0.37464 + 1.54226\kappa - 0.26992\kappa^2) \left(1 - \sqrt{T/T_c} \right) \right]^2 \quad (9)$$

$$a = 0.45724R^2T_c^2 / p_c, \quad b = 0.0778RT_c / p_c \quad (10)$$

where κ is the acentric factor given by $\kappa = 0.344$ (Yuan and Schaefer 2006), T_c is the critical temperature. In the current work, the parameter R , b , a , are given by $R = 1$, $b = 2/21$ and $a = 3/49$ (Li *et al.* 2015)

In order to achieve the wetting of solid wall and the adjustment of contact angle, in addition to the F_m , the fluid-solid pseudopotential interaction force F_b is also important, which is taken as

$$\mathbf{F}_b = -G_w \psi(x) \sum_i \omega_i \psi(x) s(\mathbf{x} + \mathbf{e}_i) \mathbf{e}_i \quad (11)$$

where $s(\mathbf{x} + \mathbf{e}_i) = 1.0$ is for solid phase, while $s(\mathbf{x} + \mathbf{e}_i) = 0$ is for fluid phase, G_w is a parameter that can align the interaction force, and ω_i are the weights, which are described as $\omega_i = w_i/3$. The buoyant force F_f is given by

$$\mathbf{F}_f = (\rho - \rho_{ave}) \mathbf{g} \quad (12)$$

where \mathbf{g} and ρ_{ave} are the gravitational acceleration and the average density among the computational domain, respectively. In the current study, an improved forcing scheme (Li *et al.* 2013) is used for the forcing term \mathbf{O} to achieve thermodynamic consistency. \mathbf{O} is given by

$$\mathbf{O} = \left[0, 6\mathbf{u} \cdot \mathbf{F} + \frac{\sigma |\mathbf{F}_m|^2}{\psi^2 \delta_t (\tau_1 - 0.5)}, -6\mathbf{u} \cdot \mathbf{F} - \frac{\sigma |\mathbf{F}_m|^2}{\psi^2 \delta_t (\tau_2 - 0.5)}, F_x, -F_x, F_y, -F_y, 2(u_x F_x - u_y F_y), u_x F_y + u_y F_x \right]^T \quad (13)$$

where parameter σ that can tune the condition of the mechanical stability is set to 1.2 (Li *et al.* 2013) for achieving the consistency of the thermodynamic.

For the solution of temperature field in the present study, the viscous heat dissipation is neglected and the target equation is taken as (Li *et al.* 2018)

$$\rho c_v (\partial_t T + \mathbf{u} \cdot \nabla T) = \nabla \cdot (\lambda \nabla T) - T \left(\frac{\partial p_{EOS}}{\partial T} \right)_\rho \nabla \cdot \mathbf{u} \quad (14)$$

where c_v and λ are the specific heat at constant volume and the thermal conductivity, respectively. The Eq. (14) can be transformed into

$$\begin{aligned} \partial_t T = & -\mathbf{u} \cdot \nabla T + \frac{1}{\rho c_v} \nabla \cdot (\lambda \nabla T) - \\ & \frac{T}{\rho c_v} \left(\frac{\partial p_{EOS}}{\partial T} \right)_\rho \nabla \cdot \mathbf{u} \end{aligned} \quad (15)$$

The Eq. (15) is solved by using FDM. The right expression of Eq. (15) is denoted by $K(T)$. The Eq. (15) is discretized in time and space. The isotropic central difference schemes (Lee and Lin 2005) are used to evaluate the spatial gradient and the Laplacian for the spatial discretization. The classical fourth-order Runge-Kutta scheme (Liu *et al.* 2013) is used for time discretization.

$$T^{t+\delta_t} = T^t + \frac{\delta_t}{6} (h_1 + 2h_2 + 2h_3 + h_4) \quad (16)$$

where $h_1, h_2, h_3,$ and h_4 are given as follows:

$$\begin{aligned} h_1 &= K(T^t) \\ h_2 &= K(T^t + 0.5\delta_t h_1) \\ h_3 &= K(T^t + 0.5\delta_t h_2) \\ h_4 &= K(T^t + \delta_t h_3) \end{aligned} \quad (17)$$

3. NUMERICAL RESULTS AND DISCUSSION

3.1 The Simulation Setup

Numerical simulations are conducted in the rectangular cavity with the calculation area of $L_x \times L_y = 450 \text{ l.u.} \times 200 \text{ l.u.}$ (l.u. represents lattice units). As shown in Fig. 1, the top and bottom of the cavity are solid walls, and the bottom wall is textured with microstructures. Figure 2 shows the different types of applicable geometry (Schubert *et al.* 2011) of the structured surface. In the present study, three structured surfaces that are close to the actual manufacturing conditions and similar to the applicable geometry of the structured surface are designed for comparison and analysis, which are defined as structure 1 (square structures), structure 2 (triangular serrated structures) and structure 3 (triangular-raised structures). The fixed width and height of the microstructure are set to 40 l.u. and 20 l.u., respectively. The spacing between the two adjacent microstructures is selected as $d = 110 \text{ l.u.}$ The bottom of the cavity and the surface of the microstructures are the heating surface. The heating surface is set as the constant temperature boundary. It should be mentioned in the current study that the conjugate heat transfer is not considered. Although there is a difference in the simulation of boiling heat transfer between using constant temperature boundary conditions and considering conjugate heat transfer, according to the conclusion drawn by (Zhao *et al.* 2019c): in the nucleate boiling stage, the difference between considering and not considering conjugate heat transfer is small, and the main difference lies in transitional boiling. The current

study is mainly concerned with the heat transfer characteristics in the nucleate boiling stage, thus, the numerical difference caused by the constant temperature boundary condition in the simulation of nucleate boiling is small. And although the constant temperature boundary condition is different from the actual condition, it can also be used to qualitatively analyze the bubble dynamics and boiling heat transfer characteristics in the boiling simulation. For example, Li obtained boiling curves (Li *et al.* 2015) and heat transfer characteristics under complex structures (Li *et al.* 2018) by using constant temperature boundary conditions in the simulation of boiling heat transfer.

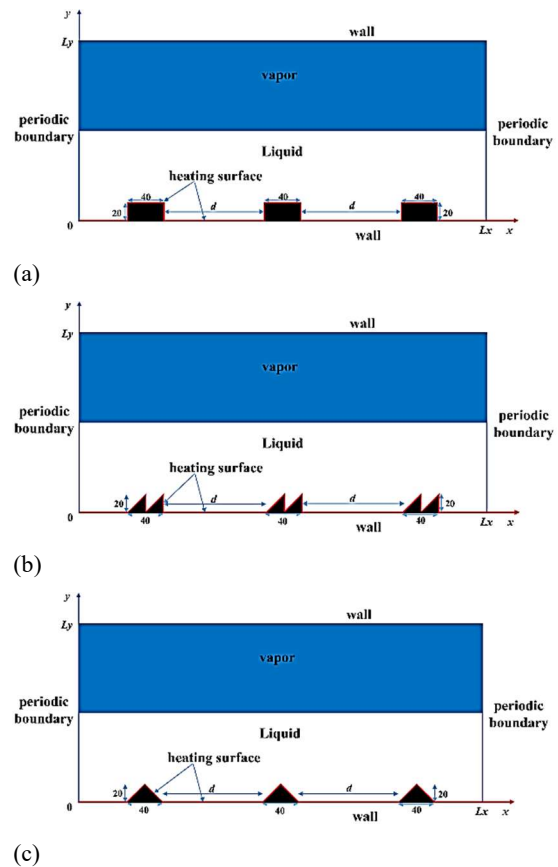


Fig. 1. Schematic diagram of structure 1(a), structure 2(b) and structure 3(c).

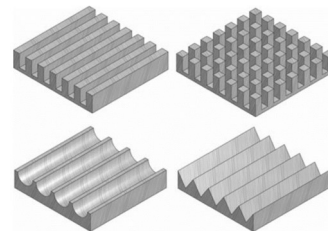


Fig. 2. Different types of applicable geometry of the structured surface.

The hydrophilic is set as the wettability of the heating surface. At the initial time, the vapor-liquid region is

divided, and the calculation area is set as liquid ($0 \leq y \leq 0.5Ly$), the remaining area is set as vapor. The temperature is set at the coexistence temperature $T_s = 0.86T_c$, at which the corresponding vapor-liquid coexistence densities are $\rho_L \approx 6.5$ and $\rho_V \approx 0.38$. The temperature on the heating surface is taken as T_b , while the top boundary temperature remains at T_s . The superheat on the heating surface is given by $\Delta T = T_b - T_s$. The *Ja* number is introduced to evaluate the degree of superheat of the heating surface, which is given by:

$$Ja = c_v(T_b - T_s)/h_{lv} \quad (18)$$

where c_v is the specific heat at constant volume, which is set to 6.0, the h_{lv} is the specific latent heat of fluid, which is determined to be 0.58 according to the literature (Gong and Cheng 2013). The formula for calculating thermal conductivity is given by $\lambda = \rho c_v \chi$, which is proportional to the density with $c_v \chi = 0.07$, where χ is the thermal diffusion coefficient. The kinematic viscosity of the liquid is set to $\nu_L = 0.1$ and the vapor is taken as $\nu_V = 0.5/3$, and the acceleration of gravity is chosen as $g = 0.00003$. For the wettability of the heating surface, the G_w is set to $G_w = 0.065$, which gives the equilibrium contact angle θ around 50° (defined in the liquid phase) at the saturation temperature. During the first 1000 time-steps, the simulations are carried out without the temperature solver. The units of all physical quantities involved in the current study are lattice units except for the dimensionless *Ja* number. It can be found from (He *et al.* 2009) that lattice units and physical units can be converted into each other.

3.2 The Boundary Settings

In the process of simulation, Zou-He non-slip boundary scheme (Zou and He 1997) is employed to the top and bottom walls: the realization of the non-slip scheme of the wall boundary lies in solving for the unknown distribution functions on the boundary. In order to achieve the non-slip boundary scheme for the wall, the velocity at the wall is set to 0, the formula $\rho u = \sum_i f_i e_i + 0.5 \delta_i F$ and $f_i - f_i^{eq} = f_{i'} - f_{i'}^{eq}$ (i' is the opposite direction of i) are used to solve for the unknown distribution functions on the wall. The periodic boundary condition is applied to the left and right boundaries. The constant temperature boundary is applied to the top and bottom walls. Since the inclination of structures 2 and 3 is 45° , the surface of structures 2 and 3 can be directly discretized to the lattice points without complicated interpolation calculations, as shown in Fig. 3. The unknown distribution functions are solved for these lattice points, which are solved by associating the two above equations and the velocity values on the boundary (the velocity is set to 0) to achieve the non-slip boundary scheme for the inclined boundaries.

3.3 Model Verification

3.3.1 D2 Law Verification

In LBM simulation of vapor-liquid phase transition, the D^2 law for describing droplet evaporation is utilized to verify the phase change model in the

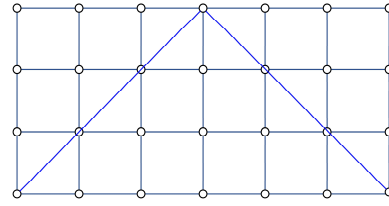


Fig. 3. Mesh discretization for inclined walls.

present study. In the initial setup, the entire computational domain is set to $200 \text{ l.u.} \times 200 \text{ l.u.}$, in which a droplet with a diameter of 60 l.u. is suspended in the central area of the calculation domain, while the rest of the domain is filled with vapor. The initial temperature in the area where the droplet is located is set to $T_s = 0.86T_c$, and the temperature in the remaining area is set to T_c , thus, the *Ja* number is equal to 0.158. The periodic boundary conditions and constant temperature boundary conditions $T = T_c$ are employed at the boundary. In the simulation of droplet evaporation, viscous heat dissipation is neglected and there is no buoyancy force. The c_v and λ are constant. The constant c_v is taken as 6.0 and the kinematic viscosity is chosen as 0.1. As shown in Fig. 4, the square of droplet diameter varies linearly with time, which conforms to the D^2 law of droplet evaporation. Therefore, the model utilized in the current study is reliable in simulating vapor-liquid phase change.

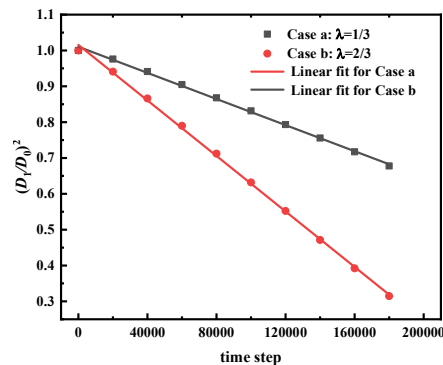


Fig. 4. D^2 law verification.

3.3.2 Simulation of Bubble Nucleation and Departure

In the process of nucleate boiling, the bubble nucleation and departure with high temperature at three grids in the bottom center wall is simulated. In the initial setting of the simulation, the grid size of $L_x \times L_y = 150 \text{ l.u.} \times 300 \text{ l.u.}$ is used in the computational domain. The calculation region of $0 \leq y \leq 0.5Ly$ is liquid, and the remaining domain is vapor. The kinematic viscosity is taken as 0.1, The constant c_v is taken as 5.0, and the thermal diffusivity is chosen as 0.06. Except that the temperature of the three center grids is fixed to high temperature $T_h = 1.25T_c$, the temperature of the bottom wall is fixed to $T_s = 0.86T_c$, and the initial temperature of the rest of the domain is taken as T_s , thus, the *Ja* number is

equal to 0.44. The equilibrium contact angle is taken as $\theta \approx 45^\circ$. The periodic boundary conditions are employed at the left and right sides of the computational domain. As shown in Fig. 5, the bubble departure diameter obtained in the current study is proportional to $g^{-0.5}$, which satisfies the relationship obtained in the literature (Friz 1935). Therefore, it fully shows that the phase change model adopted in the present study has excellent reliability in simulating boiling.

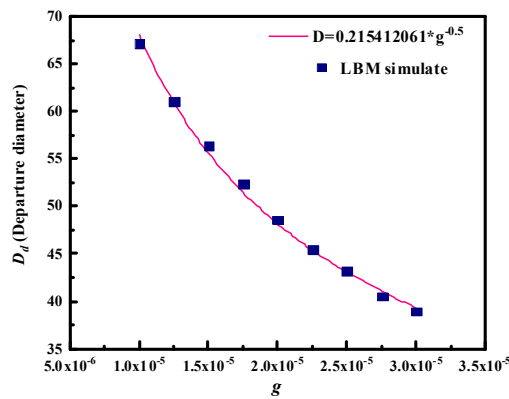


Fig. 5. The effect of gravity on bubble departure diameter.

3.4 The Effects of Microstructure Geometry on Bubble Dynamics Behavior and BHT Characteristics

In the current study, three different kinds of structured surfaces are used to study the effects of microstructure geometry on bubble dynamic and heat transfer characteristics, namely structure 1, structure 2, structure 3. Figures 6 and 7 show a comparison of the average heat flux and heat transfer coefficient on the surface of structures 1, 2 and 3 during nucleate boiling, respectively. Each point in Fig. 6. represents the average heat flux of the heating surface at such Ja number, which is the time average of the transient heat flux during the time steps of 1000 to 40000, and the transient heat flux is the spatial average of the local heat flux along the heating surface, and the local heat flux is calculated by Fourier heat conduction law. The heat transfer coefficient is defined as the average heat flux divided by superheat. According to the above definition, the average heat flux and heat transfer coefficient are calculated as:

$$Q_{ave} = \int_{1000}^{40000} \left(\int_0^{L_w} (-\lambda \partial T / \partial y) dx / L_w \right) dt / 39000 \quad (19)$$

$$J = Q_{ave} / \Delta T \quad (20)$$

where Q_{ave} is the average heat flux, J is the heat transfer coefficient, L_w is the total length of heating surface.

It can be seen from figures 6 and 7 that the average heat flux and heat transfer coefficient on the surface of structure 1 are higher than those of structures 2

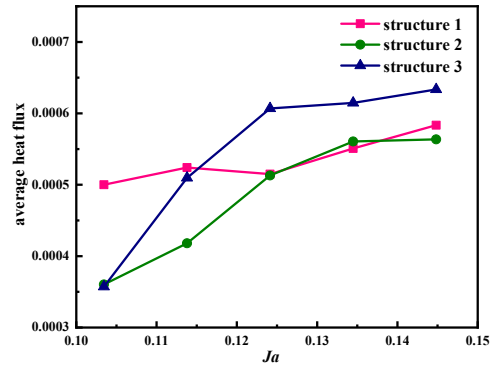


Fig. 6. Comparison of average heat fluxes on three kinds of structured surfaces under different Ja number.

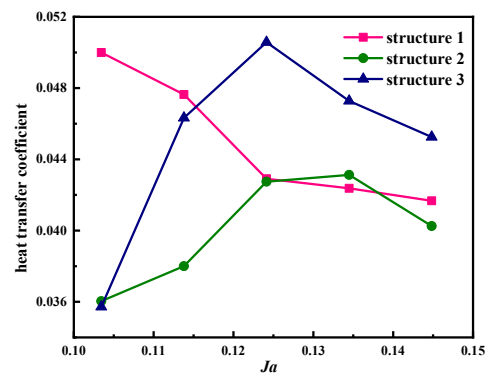


Fig. 7. Comparison of the heat transfer coefficient on three kinds of structured surfaces under different Ja number.

and 3 at the initial stage of nucleate boiling ($Ja = 0.103$ and $Ja = 0.114$), thus, the performance of BHT is better. This is because the bottom corner of the columnar structure accelerates the nucleation of bubbles, and the top corner effect leads to the growth pattern of bubbles expanding, contracting, and pulling up on both sides of the structure, as shown in Fig. 8. This growth model leads to the enhancement of the disturbance to the flow field and the convection on the flat surface. Figures 6 and 7 also show that the average heat flux and heat transfer coefficient on the surface of structure 2 are almost smaller than those of structures 1 and 3. The reason is that in the nucleate boiling process, the nucleated and growing bubbles in the central groove of structure 2 do not break away from the wall with the separation of the merged bubbles, and remain in the grooves all the time, as shown in Fig. 9. Thus, this accelerates the process of bubble coalescence, and because the bubbles always cover the heating surface in the grooves, the BHT in the grooves deteriorates. Therefore, the BHT performance of structure 2 is almost weaker than that of structures 1 and 3 during nucleate boiling.

When the Ja number is 0.124-0.145, nucleate boiling has been fully developed, Fig. 6 shows that the average heat flux on the structure 3 surface is larger than those of structures 1 and 2, and it is most evident

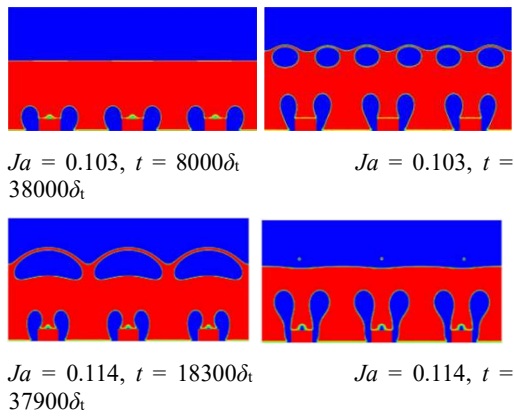


Fig. 8. Snapshots of the process of boiling on structure 1 surface at $Ja = 0.103$ and $Ja = 0.114$.

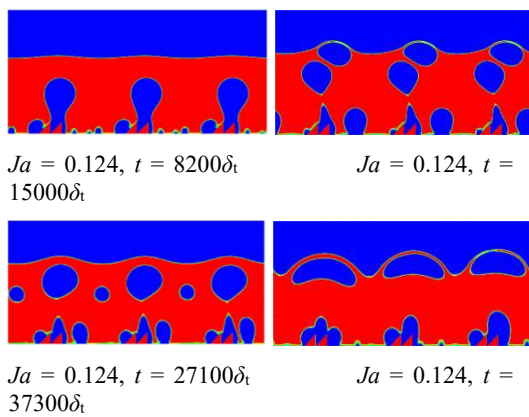


Fig. 9. Snapshots of the process of boiling on structure 2 surface at $Ja = 0.124$.

when the Ja number is 0.124. The heat transfer coefficient curve shows that when the Ja number is 0.124, the BHT efficiency on the structure 3 surface is the highest among all three. Therefore, in the current study, we focus on the analysis of the boiling phenomenon and BHT characteristics on the structured surface when the Ja number is 0.124. Fig. 10 shows the time evolution of transient heat fluxes on different structured surfaces. Compared with the boiling phenomenon between adjacent time-steps marked in the diagram, it can be found that the variation of heat flux at each time in the diagram is related to the motion of bubbles. Therefore, based on the motion of bubbles, the present study deeply explores the boiling heat transfer mechanism of three kinds of structured surfaces. From the boiling phenomenon in Fig. 11(a-c), it can be observed that for three kinds of structural surfaces, whenever bubbles expand on the heating surface and merge with each other during bubble nucleation and growth, these lead to the decline of the heat flux curve, resulting in the weakening of the BHT performance. On the other hand, whenever the growing and merged bubbles shrink, deform and detach on the heating wall, these lead to the upward movement of the heat flux curve, thus enhancing the BHT performance.

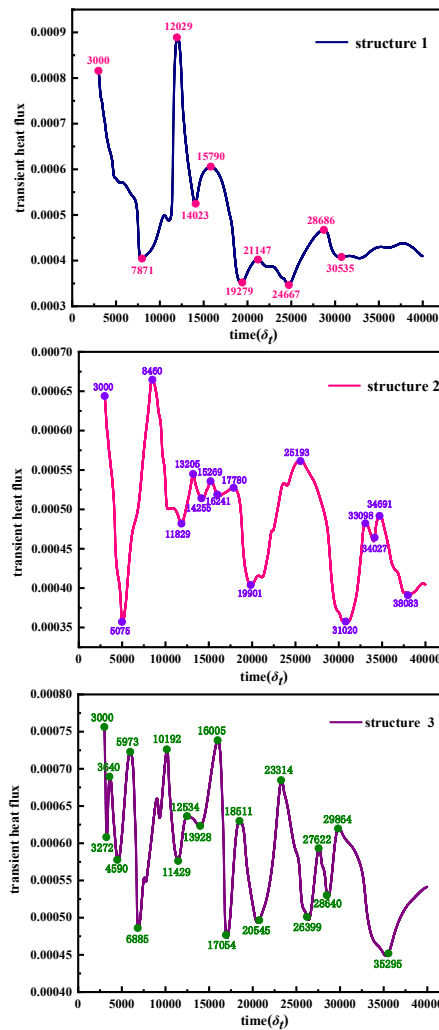


Fig. 10. Time evolution of transient heat fluxes on structures 1, 2 and 3 surfaces at $Ja = 0.124$.

During the boiling process in structures 2 and 3, a special bubble motion behavior is found to enhance BHT. Due to the inclined protruding structure in structures 2 and 3 and the flow field disturbance caused by the oscillation and deformation of the merged bubble in the process of gradually detaching from the wall, the continuous nucleation of small bubbles on the heating surface and the movement behavior of bubbles lateral migration are produced, as shown in Fig. 11(b, c). This process enhances the heat transfer performance. Therefore, combined with the above bubble dynamic behavior analysis, the bubble necking, deformation, detachment process and the movement behavior of bubbles lateral migration on the heating wall make the heating wall wetted again, thus enhancing the transient heat conduction of the superheated layer around the boiling site of the rewetting wall. At the same time, the growth, oscillation and detachment of bubbles also perturb the liquid and enhance the natural convection around the bubbles. This part of the enhanced convection around the bubble is called micro-convection. Therefore, in the present study, the main heat transfer mechanism of nucleate boiling on the three kinds of structured surface is the

combined action of transient heat conduction and micro-convection. Because the bubbles located in the region between the two adjacent microstructures in structure 1 merge to form a large bubble after 15800 time steps, the vapor film remains on the flat surface all the time after the bubble detaches, as shown in Fig. 11(a). The BHT performance is weakened. On the other hand, the heat transfer performance of structure 2 is weakened because there are always bubbles in the central groove during the whole boiling process. The structure 3 has the best heat transfer performance due to its special structure, which accelerates the process of frequent necking and detachment of the merged bubbles from the wall and strengthens the lateral migration behavior of the bubbles, as shown in Fig. 11(c).

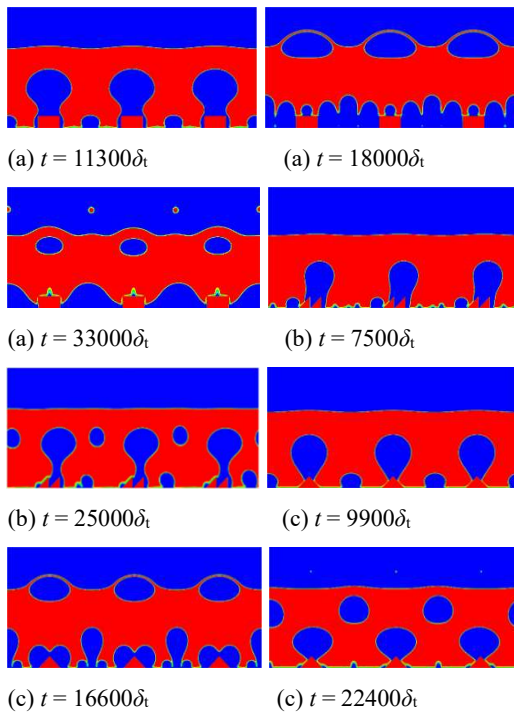


Fig. 11. Snapshots of the process of boiling on structure 1(a), structure 2(b) and structure 3(c) surfaces at $Ja = 0.124$.

3.5 The Effects of Spacing Between Microstructures on Bubbles Nucleation and BHT Characteristics

Since that structure 3 shows better BHT performance in the process of nucleate boiling, and that the heat flux and heat transfer coefficient are higher than those of structures 1 and 2, structure 3 is used in the present study as the benchmark model to study the effects of the spacing between microstructures on bubble dynamics and BHT characteristics. In the current study, the effect of the spacing between microstructures on bubbles nucleation is discussed, and the motion behavior of bubbles and heat transfer characteristics with different spacing are analyzed emphatically when the Ja number is 0.124. The distance between the microstructures is set to 0, 22,

44, 66, 88, 110 l.u. Fig. 12 shows that the average heat flux varies with the distance between the microstructures when the Ja number is 0.124, 0.134, 0.145. The average heat flux fluctuates with the increase of the distance between microstructures. Therefore, the variation of the spacing between microstructures has an important effect on the BHT performance of the heating surface.

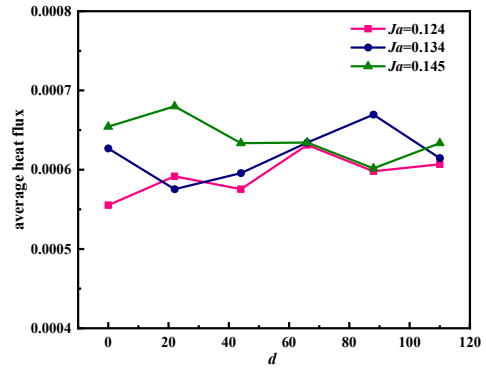


Fig. 12. Variation of the average heat fluxes with the distance between the microstructures at $Ja = 0.124, 0.134, 0.145$.

Figure 13 depicts the distribution of time-averaged local heat flux on the heating surface when the Ja number is 0.124 and the spacing is 0, 22, 44, 66, 88, 110 l.u., respectively. The time-averaged local heat flux is the time average of the local heat flux during the time steps of 1000 to 40000. Figure 13 shows that the time-averaged local heat flux fluctuates on the heating surface, with multiple peaks and troughs. The trough represents the small time-averaged local heat flux in the region, which indicates that nucleating bubbles are often produced in the region. Therefore, it can be determined that this area is the main region of activation nucleation sites for producing bubbles. It can be seen from the Fig. 13 that the regions 1, 2 and 3 marked in the graph are in the trough of the curve with the time-averaged local heat flux being the smallest. Therefore, it can be explained that bubbles are often produced in these regions – the main nucleation region. By obtaining the coordinates of the points of the smallest time-averaged local heat flux corresponding to the curve of each interval, it can be found that the coordinates exactly correspond to the intersection of the microstructure and the bottom wall. Therefore, the existence of microstructure accelerates the bubble nucleation, making the bottom corner the easiest and the fastest point to produce nucleating bubbles.

It can be seen from the Fig. 13 that when the distance between the microstructures increases from 0 to 22, the region between the 1 and 2 in the figure does not produce the activated nucleation sites of bubbles. As the spacing increases to 44, nucleation points begin to appear in the center of the region between the 1 and 2, and when the spacing increases to 66, two main bubble activation nucleation regions 6 and 7 develop. The activated nucleation sites of bubbles are mainly formed in these two regions. As the

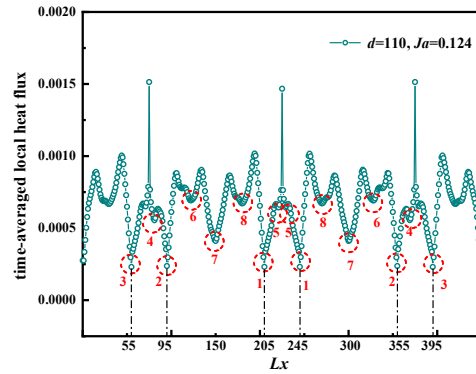
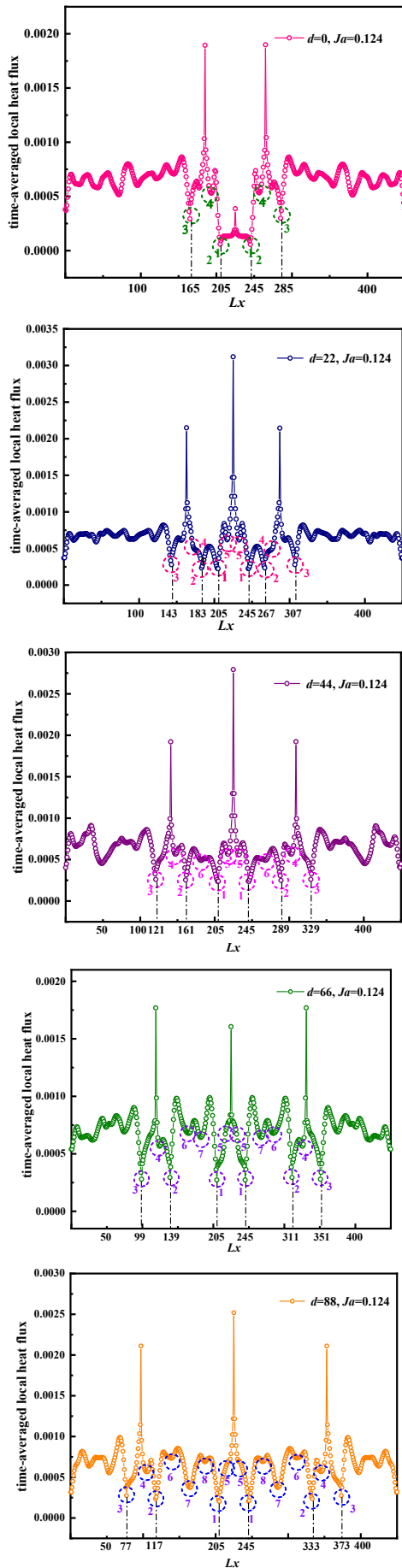


Fig. 13. Distribution of time-averaged local heat flux on the structure 3 surface at $Ja = 0.124$ and $d = 0, 22, 44, 66, 88, 110$.

distance between microstructures continues to increase, the bubble activated nucleation region 8 is increased, and as the spacing increases to 110, the 6, 7 and 8-nucleation regions all develop, and they produce more activated nucleation sites, while the bubble 7-nucleation region in the center develop into the main bubble nucleation region with its bubble nucleation rate being significantly faster than that of the 6 and 8-regions. The spacing between the microstructures not only affects the generation of nucleation points in the the region between the 1 and 2, but also has an important influence on the location of bubble activation nucleation on the surface of the microstructure, such as the 4, 5-nucleation regions marked in the figure. Therefore, the variation of the distance between microstructures has an important effect on the generation of activated nucleation sites on the heating surface.

3.6 The Effects of Spacing Between Microstructures on Bubble Dynamic Behavior

In the current study, in addition to analyzing the effect of the spacing between microstructures on the nucleation of bubbles on the heating surface, the effect of the spacing between microstructures on the bubbles dynamic behavior is also discussed when the Ja number is 0.124. When the distance between the microstructures is 0, by observing the boiling process described by Fig. 14(a), the regions where the bubbles merge and detach are mainly on the three structured surfaces and the left and right boundaries. However, during the whole boiling process, the surface of the microstructure in the middle position is always covered with a vapor film, so this leads to the deterioration of heat transfer. Due to the disturbance of the flow field and the special microstructure of structure 3, it can be observed that the nucleation bubbles near the surface of the microstructure migrate to the structured surface and the bubbles near the left or right boundary of the computational domain migrate to the left or right boundary, as shown in Fig. 14(a). As the spacing increases to 22, the boiling process described by Fig. 14(b) shows that the main merging region of the bubble changes, and the bubble merging and detaching no longer occurs on the structured surface

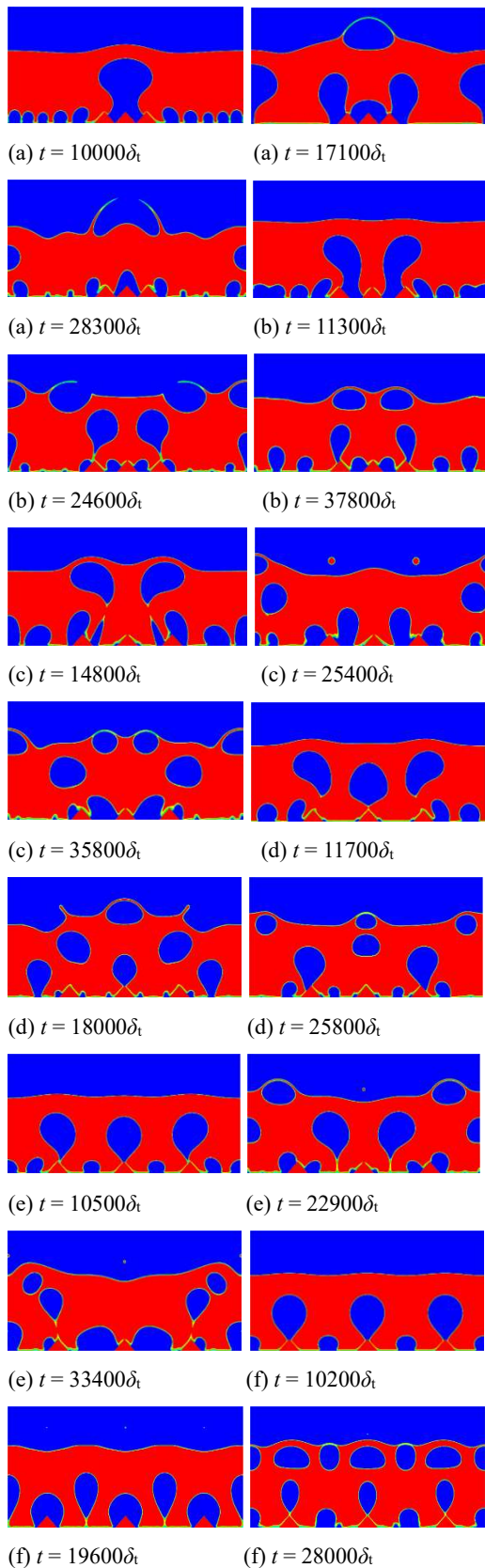


Fig. 14. Snapshots of the process of boiling on structure 3 surface at $Ja = 0.124$ and $d = 0$ (a), 22(b), 44(c), 66(d), 88(e), 110(f).

of the middle region. The bubble coalescence and detachment mainly occur on the left and right

structured surface and the left and right boundary, but the bubbles lateral migration phenomenon does not change. When the distance between the microstructures increases to 44, Fig. 14(c) shows that the main areas of bubble merging and detaching extend from the left and right sides of the structured surface to the flat surface between the microstructures, while the other ones remain unchanged. However, when the spacing continues to increase to 66, not only the main areas of bubble merging and detachment have changed, but also the lateral migration direction of bubbles has changed. The main areas where bubbles merge and detach occur on all the structured surfaces, and the lateral migration direction of the bubbles nucleated on the flat surface moves toward the inclined surface of the microstructure, as shown in Fig. 14(d). As the distance between the microstructures continues to increase, Fig. 14(e, f) shows that the main regions of bubble merging and detaching occur not only on the surfaces of all microstructures, but also on the region center between the microstructures and on the left and right boundaries. The number of times of lateral migration of bubbles decreases with the increase of the spacing.

The bubbles dynamic behavior on the heating surface has an important effect on the BHT performance in nucleate boiling. As shown in Fig. 12, when the Ja number is 0.124, the BHT performance is the best as the spacing increases to 66, because the microstructure of structure 3 accelerates the frequent necking, deformation, and detachment of the merged bubbles compared with the flat surface, and strengthens the movement behavior of the bubbles lateral migration and the continuous nucleation process of the small bubbles on the heating surface. Such series of bubble dynamic behaviors enhance the transient heat conduction and micro-convection, with the strongest effect achieved when the distance between the microstructures is 66, because when the spacing is 66, the main area of bubble merging and detaching is on the surface of the microstructure, the movement behavior of the bubbles lateral migration is frequent, and the lateral migration direction always moves to the inclined surface of the microstructure, as shown in Fig. 14(d). Therefore, bubble merging, necking, deformation and detachment on the structured surface accelerate, as well as the continuous nucleation of small bubbles on the heating surface.

4. CONCLUSION

In the current study, the pseudopotential multiphase LB model coupled FDM is used to simulate the pool boiling process and enhanced BHT characteristics on the structured surface. The effects of microstructure geometry and spacing on BHT characteristics and bubble dynamics behavior are studied in detail. Through our simulation study, the following main conclusions and findings are obtained.

The heat transfer performance of structure 1 is better than those of structures 2 and 3 at the initial stage of nucleate boiling (Ja number is 0.103-0.114). The heat transfer performance of structure 2 is almost weaker than those of structures 1 and 3 during

nucleate boiling. The boiling heat transfer performance of structure 3 is significantly better than those of structures 1 and 2 in the nucleate boiling (*Ja* number is 0.124-0.145).

On the three kinds of structured surfaces, when the bubbles expand on the heating surface and merge with each other during bubble nucleation and growth, the heat transfer performance is weakened. On the other hand, when the growing and merged bubbles shrink, deform and detach on the heating wall, the BHT performance is enhanced.

During the boiling process of structures 2 and 3, the continuous nucleation of small bubbles and the motion behavior of bubbles lateral migration caused by the oscillation and deformation of the merged bubbles are found. Such behaviors enhance the BHT performance. Most BHT is due to the re-wetting of the heating surface during bubble necking, deformation, detachment, and lateral migration, as well as enhanced convection around bubbles during bubble growth, oscillation and detachment, which indicates that the main BHT mechanism of nucleate boiling on the three kinds of structured surface is the combined action of transient heat conduction and micro-convection.

The variation of the distance between the microstructures has an important effect on the BHT performance of the heating surface. Moreover, the variation of the distance between the microstructures has an important influence on the generation of the activated nucleation sites on the heating surface. The existence of the microstructure accelerates the bubble nucleation, making the bottom corner the easiest and the fastest point to produce nucleating bubbles.

In the nucleate boiling stage, compared with the flat surface, the microstructure of structure 3 accelerates frequent necking, deformation and detachment of the merged bubbles from the heating wall, and strengthens the movement behavior of the bubbles lateral migration and the continuous nucleation of small bubbles on the heating surface. Therefore, structure 3 can enhance the transient heat conduction and micro-convection. The bubble dynamics behavior of the heating surface shows that the strengthening effect is the strongest as the spacing increases to 66 when the *Ja* number is 0.124.

ACKNOWLEDGEMENT

Financial grants were received from the National Natural Science Foundation of China (11562011 and 51566012), Natural Science Foundation of Jiangxi Province of China (20181BAB206031), De Montfort University through its distinguished Vice-Chancellor 2020 Programme, and the UK Science and Technology Facilities Council (STFC) through Batteries Early Career Researcher Award. Their support is greatly appreciated by the authors.

REFERENCES

Bi, J., D. M. Christopher, D. Zhao, J. Xu and Y.

Huang (2019). Numerical study of bubble growth and merger characteristics during nucleate boiling. *Progress in Nuclear Energy* 112, 7-19.

Chang, X., H. Huang, Y. P. Cheng and X. Y. Lu (2019). Lattice Boltzmann study of pool boiling heat transfer enhancement on structured surfaces. *International Journal of Heat and Mass Transfer* 139, 588-599.

Chu, K. H., R. Enright and E. N. Wang (2012). Structured surfaces for enhanced pool boiling heat transfer. *Applied Physics Letters* 100(24), 241603.

Dhir, V. K., G. R. Warrier and E. Aktinol (2013). Numerical simulation of pool boiling: a review. *Journal of Heat Transfer* 135(6).

Dong, B., Y. Zhang, X. Zhou, C. Chen and W. Li (2020). Numerical simulation of bubble dynamics in subcooled boiling along inclined structured surface. *Journal of Thermophysics and Heat Transfer* 35(1), 16-27.

Friz, W. (1935). Maximum volume of vapor bubbles. *Physic. Zeitsch.* 36, 379-354.

Gong, S. and P. Cheng (2013). Lattice Boltzmann simulation of periodic bubble nucleation, growth and departure from a heated surface in pool boiling. *International Journal of Heat and Mass Transfer* 64, 122-132.

Halon, T., B. Zajackowski, S. Michaie, R. Rulliere and J. Bonjour (2018). Enhanced tunneled surfaces for water pool boiling heat transfer under low pressure. *International Journal of Heat and Mass Transfer* 116, 93-103.

Hamzekhani, S., M. M. Falahieh, M. R. Kamalizadeh and M. Salmaninejad (2015). Bubble dynamics for nucleate pool boiling of water, ethanol and methanol pure liquids under the atmospheric pressure. *Journal of Applied Fluid Mechanics* 8(4), 893-898.

He, Y.L., Y. Wang and Q. Li (2009). *Lattice Boltzmann method: theory and applications*. Science, Beijing.

Jo, H., H. S. Ahn, S. Kang and M. H. Kim (2011). A study of nucleate boiling heat transfer on hydrophilic, hydrophobic and heterogeneous wetting surfaces. *International Journal of Heat and Mass Transfer* 54(25-26), 5643-5652.

Kim, D. E., D. I. Yu, D. W. Jerng, M. H. Kim and H. S. Ahn (2015a). Review of boiling heat transfer enhancement on micro/nanostructured surfaces. *Experimental Thermal and Fluid Science* 66, 173-196.

Kim, S. H., G. C. Lee, J. Y. Kang, K. Moriyama, M. H. Kim and H. S. Park (2015b). Boiling heat transfer and critical heat flux evaluation of the pool boiling on micro structured surface. *International Journal of Heat and Mass Transfer* 91, 1140-1147.

Lee, T. and C. L. Lin (2005). A stable discretization

- of the lattice Boltzmann equation for simulation of incompressible two-phase flows at high density ratio. *Journal of Computational Physics* 206(1), 16-47.
- Li, Q., K. H. Luo and X. J. Li (2013). Lattice Boltzmann modeling of multiphase flows at large density ratio with an improved pseudopotential model. *Physical Review E* 87(5), 053301.
- Li, Q., Q. J. Kang, M. M. Francois, Y. L. He and K. H. Luo (2015). Lattice Boltzmann modeling of boiling heat transfer: The boiling curve and the effects of wettability. *International Journal of Heat and Mass Transfer* 85, 787-796.
- Li, Q., Y. Yu, P. Zhou and H. J. Yan (2018). Enhancement of boiling heat transfer using hydrophilic-hydrophobic mixed surfaces: a lattice Boltzmann study. *Applied Thermal Engineering* 132, 490-499.
- Liu, H., A. J. Valocchi, Y. Zhang and Q. Kang (2013). Phase-field-based lattice Boltzmann finite-difference model for simulating thermocapillary flows. *Physical Review E* 87(1), 013010.
- O'hanley, H., C. Coyle, J. Buongiorno, T. Mckrell, L. W. Hu, M. Rubner and R. Cohen (2013). Separate effects of surface roughness, wettability, and porosity on the boiling critical heat flux. *Applied Physics Letters* 103(2), 024102..
- Schubert, A., M. Hackert-Oschätzchen, G. Meichsner and M. Zinecker (2011). Design and realization of micro structured surfaces for thermodynamic applications. *Microsystem technologies* 17(9), 1471-1479.
- Tang, Y., J. Zeng, S. Zhang, C. Chen and J. Chen (2016). Effect of structural parameters on pool boiling heat transfer for porous interconnected microchannel nets. *International Journal of Heat and Mass Transfer* 93, 906-917.
- Thiagarajan, S. J., R. Yang, C. King and S. Narumanchi (2015). Bubble dynamics and nucleate pool boiling heat transfer on microporous copper surfaces. *International Journal of Heat and Mass Transfer* 89, 1297-1315.
- Wei, J.J., L. J. Guo and H. Honda (2005). Experimental study of boiling phenomena and heat transfer performances of FC-72 over micro-pin-finned silicon chips. *Heat and Mass Transfer* 41(8), 744-755.
- Xie, S., Q. Tong, Y. Guo, X. Li, H. Kong and J. Zhao (2020). The effects of surface orientation, heater size, wettability, and subcooling on the critical heat flux enhancement in pool boiling. *International Journal of Heat and Mass Transfer* 149, 119230.
- Xie, S., M. Jiang, H. Kong, Q. Tong and J. Zhao (2021a). An experimental investigation on the pool boiling of multi-orientated hierarchical structured surfaces. *International Journal of Heat and Mass Transfer* 164, 120595.
- Xie, S., X. Ma, H. Kong, S. Bai, M. Jiang and J. Zhao (2021b). The synergetic effects of the surface wettability and the patterned nanostructure on boiling heat transfer enhancement. *International Journal of Heat and Mass Transfer* 176, 121475.
- Yuan, P. and L. Schaefer (2006). Equations of state in a lattice Boltzmann model. *Physics of Fluids* 18(4), 042101.
- Zhang, Y., J. Bao, M. Yao, Y. Xie, Y. Huang and P. Li (2020). Non-orthogonal Multiple-Relaxation-Time Lattice Boltzmann Simulation of Mixed Convection in Lid-Driven Porous Cavity with an Isothermally Heated Block. *Journal of Applied Fluid Mechanics* 13(5).
- Zhao, W., J. Liang, M. Sun, X. Cai and P. Li (2019a). Hybrid phase-change lattice Boltzmann simulation of the bubble nucleation and different boiling regimes of conjugate boiling heat transfer. arXiv preprint arXiv:1911.10747.
- Zhao, W., Y. Zhang and B. Xu (2019b). An improved pseudopotential multi-relaxation-time lattice Boltzmann model for binary droplet collision with large density ratio. *Fluid Dynamics Research* 51(2), 025510.
- Zhao, W., J. Liang, M. Sun and Z. Wang (2021c). Investigation on the effect of convective outflow boundary condition on the bubbles growth, rising and breakup dynamics of nucleate boiling. *International Journal of Thermal Sciences* 167, 106877.
- Zhao, W., Y. Zhang, W. Shang, Z. Wang, B. Xu and S. Jiang (2019). Simulation of droplet impacting a square solid obstacle in microchannel with different wettability by using high density ratio pseudopotential multiple-relaxation-time (MRT) lattice Boltzmann method (LBM). *Canadian Journal of Physics* 97(1), 93-113.
- Zhou, P., W. Liu and Z. Liu (2019). Lattice Boltzmann simulation of nucleate boiling in micro-pillar structured surface. *International Journal of Heat and Mass Transfer* 131, 1-10.
- Zonouzi, S. A., H. Safarzadeh, H. Aminfar and M. Mohammadpourfard (2018). Experimental study of subcooled boiling heat transfer of axial and swirling flows inside mini annular gaps. *Journal of Applied Fluid Mechanics* 11(1), 225-232.
- Zou, Q. and X. He (1997). On pressure and velocity boundary conditions for the lattice Boltzmann BGK model. *Physics of Fluids* 9(6), 1591-1598.